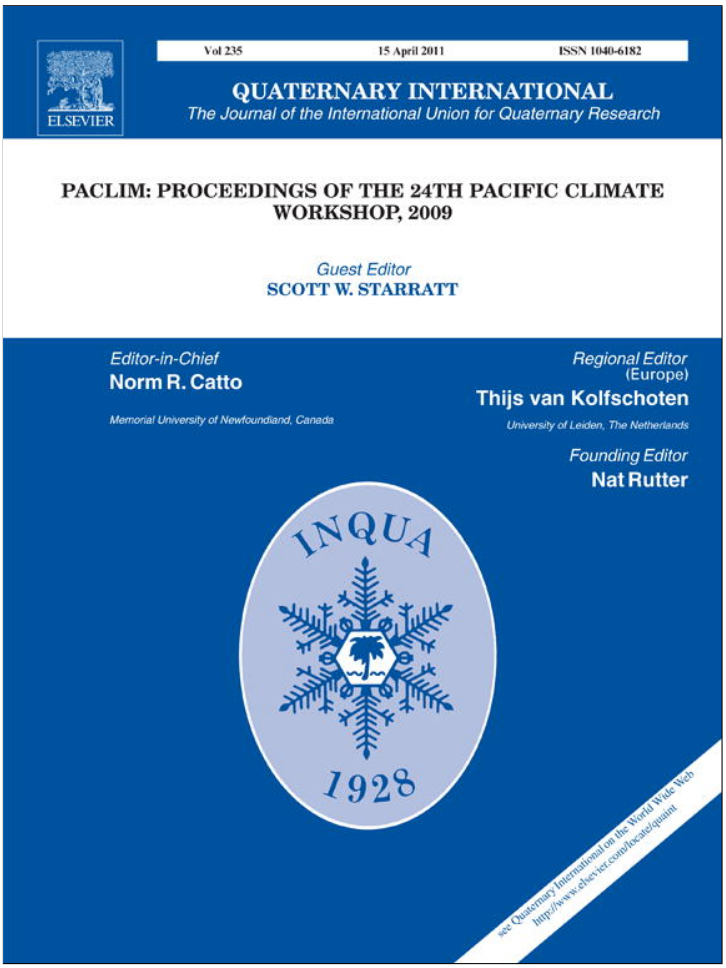

Quaternary International 235 (2011) 89–100

Contents lists available at ScienceDirect

Quaternary International

journal homepage: www.elsevier.com/locate/quaint

Inferring precipitation-anomaly gradients from tree rings

David M. Meko [a,*], David W. Stahle [b], Daniel Griffin [a], Troy A. Knight [a,1]

[a] Laboratory of Tree-Ring Research, University of Arizona, 105 W Stadium, Tucson, AZ 85721, United States
[b] Department of Geosciences, University of Arkansas, Fayetteville, AR, United States

ARTICLE INFO

Article history:
Available online 22 September 2010

ABSTRACT

Long-term information on gradients in precipitation-anomaly over tens to hundreds of km is important to hydroclimatology for improved understanding of the spatiotemporal variability of moisture-delivery systems and runoff. Site-centered reconstructions of cool-season (Nov–Apr) precipitation at 36 *Quercus douglasii* tree-ring sites in the Central Valley of California, USA, are generated, regionalized, and evaluated for ability to track north–south gradients in precipitation-anomaly. Event series are constructed for overall-wet (W), overall-dry (D), wetter-to-north (W/D) and wetter-to-south (D/W) conditions, 1557–2001. Interesting features of the event series are clustering of W events in the 1780–1790s and a three-year run of D/W events in 1816–1818 (coincidentally following the eruption of Tambora in 1815). The most recent 25 years of the event series stand out for a high frequency of W and D events and low frequency of events associated with strong gradients in precipitation-anomaly. The five strongest W events in this period and seven of the nine W events since 1934 match El Niño years. Recent changes in the event series may be a Central-Valley footprint of a well-documented post-1976 change in the atmosphere-ocean climate system over the North Pacific. Similar studies may prove useful in other geographical areas where networks of tree-ring data sufficiently sensitive to precipitation are available.

1. Introduction

Although tree-ring data have been widely used for climate reconstruction on various spatial scales (Fritts, 1976, 1991; Hughes et al., 1982; Stockton et al., 1985), little attention has been directed to the ability of a densely sampled network of tree-ring data to capture patterns of moisture-anomaly gradients over distances of just a few hundred kilometers. A change in moisture-anomaly gradient over time at this spatial scale might reflect changes in predominant positioning of ridges and troughs, or shifts in storm tracks. Such a change could also indicate modulation of the regional climate signal related to ocean-atmosphere forcings, such as El Niño/Southern Oscillation (ENSO). Spatially-resolved moisture anomalies from tree rings could, for example, shed light on long-term variability of the latitude of the pivot point, identified near 40° N, in ENSO-related precipitation anomalies along the West Coast and western cordillera of North America (Dettinger et al., 1998; Wise, 2010).

Information on changes in moisture-anomaly gradients could be useful in water-resources research for evaluating the susceptibility of water supply to runoff anomalies in tributary watersheds. The ability of runoff surpluses in some tributaries to offset deficits in others, for example, is an important question in water-supply management in large basins such as the Colorado and Sacramento in the western USA (e.g., Jones, 2008). The large-scale gridded (2.5° × 2.5°) climate reconstructions of the North American Drought Project (NADP) (Cook et al., 1999, 2004) demonstrate that spatial fields of anomalies in drought-related climate variables can be inferred from tree-ring networks. The interest in this paper is in moisture-anomaly gradients at the spatial scale of a few hundred km for a specific season such that tree-ring results can be directly tied to seasonal moisture-delivery systems of the atmosphere.

A collection of blue oak (*Quercus douglasii*) from the Central Valley of California and surrounding areas is analyzed in this paper for strength of signal for cool-season (Nov–Apr) precipitation and for ability to track temporal variations in north/south gradient of precipitation-anomaly. A network of 36 chronologies is first converted to estimates of cool-season precipitation at each site. The site-centered precipitation series are then grouped into North, Central and South regions. Regional-average series are tested for relationship with observed precipitation, with a focus on events: 1) dry overall, 2) wet overall, 3) wetter-to-north, and 4) wetter-to-south. Time series of events are then tallied and examined for long-term changes in frequency of events. Events are related to 500 mb height anomalies, El Niño/La Niña occurrence, and drought-index spatial patterns over western North America.

* Corresponding author. Fax: +1 520 621 8229.
E-mail address: dmeko@LTRR.arizona.edu (D.M. Meko).
[1] Present address: Environmental Studies Program, College of Saint Benedict, St. Joseph, MN 56374, United States.

1040-6182/$ – see front matter © 2010 Elsevier Ltd and INQUA. All rights reserved.
doi:10.1016/j.quaint.2010.09.006

2. Study area and data

The study area is the Central Valley of California and surrounding locations in the foothills of the Sierra Nevada Mountains and coastal ranges. The area encompasses parts of the Cascade-Sierra Mountains and Pacific Border physiographic provinces and includes one of the most productive agricultural regions in the world (Crippen, 1986). The climate is Mediterranean-type, with dry summers, mild wet winters, and precipitation mostly from cyclonic storms imbedded in the westerlies (Baldwin, 1973). Snow is increasingly important to the annual precipitation regime toward the higher elevations of the Sierra Nevada (Cayan, 1996).

The primary tree-ring data, developed by researchers from the University of Arkansas Tree-Ring Laboratory, consists of 36 *Q. douglasii* residual site chronologies from the Central Valley of California and nearby locations (Fig. 1). Residual chronologies are averages over many trees of autoregressive (AR) residuals from low-order AR models fit to individual detrended ring-width series (Cook, 1985; Cook et al., 1990). (Chronologies generated without the step of AR modeling are referred to as standard chronologies.) Residual chronologies are sometimes preferred over standard chronologies as predictors in dendroclimatic reconstruction models because standard chronologies may contain persistence associated with food-storage carryover and other non-climatic factors (Fritts, 1976; Cook, 1985).

Each site's tree-ring specimens were non-destructively collected, prepared and analyzed by methods standard in dendrochronology (Stokes and Smiley, 1996). The calendar year of formation of each ring was determined by cross-dating (Douglass, 1941), and ring widths were measured to a precision of 0.001 mm under the microscope with a Velmex stage micrometer. Calendar-year dating and measurement accuracy were verified with program COFECHA (Holmes, 1983; Grissino-Mayer, 2001). Site-level residual chronologies were computed using program ARSTAN (Cook, 1985; Cook et al., 1990) to double-detrend (Holmes et al., 1986) the time series of ring-width measurements, model and remove the low-order persistence theorized to result from biological memory, and robustly average the derived ring-width indices into site chronologies. Each chronology includes at least 40 living trees, and the average number of living trees and dead stems is 65 per collection site. Time coverage varies from site-to-site: starting year ranges from 1293 to 1808, and ending year from 1996 to 2005. All except two of the chronologies are complete through at least the 2003 ring. The ring-width measurements and chronologies are available from the International Tree-Ring Data Bank (http://www.ncdc.noaa.gov/paleo/treering.html). The tree-ring sites, measurements, and steps in chronology development are described in more detail in Stahle et al. (in press) and in the Supplementary Data. The chronologies have previously been applied in reconstruction of various quantities, including the salinity gradient in an estuary of San Francisco Bay (Stahle et al. (in press)), streamflow (Meko et al., 2001; Griffin, 2007), and salinity (Stahle et al., 2001).

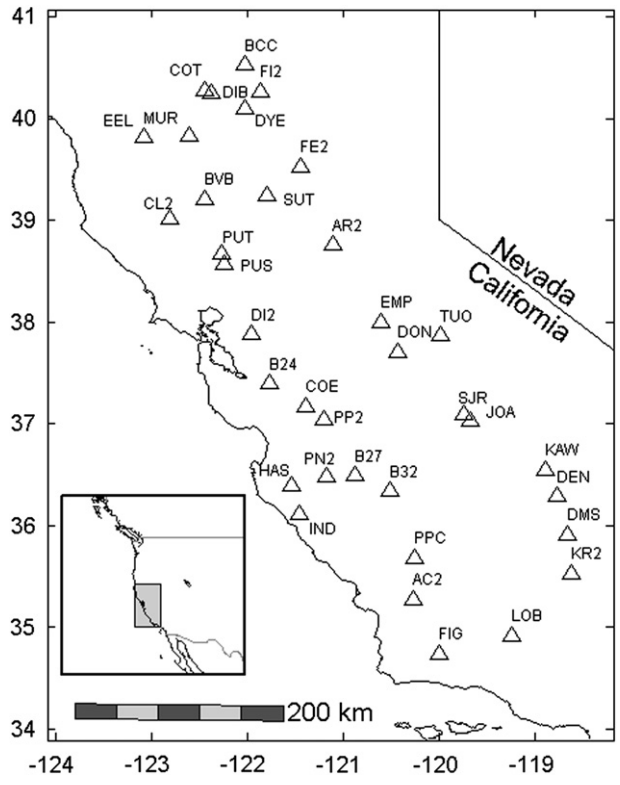

Fig. 1. Map showing locations of tree-ring sites. Site codes follow Table 1.

Interpolated monthly precipitation at the latitude-longitude coordinates of each of the 36 tree-ring sites was downloaded from the Website of the PRISM Climate Group, Oregon State University (http://www.prismclimate.org, data created July 12, 2008). PRISM stands for "Parameter-elevation Regressions on Independent Slopes Model"; the data are the result of an interpolation from station climate series specifically screened for climatological studies (Daly et al., 2002, 2008; Gibson et al., 2002). PRISM data was preferred over individual-station data for this study because the tedious process of quality control, assimilation of records from various networks, and spatial interpolation (4 km grid) has already been done. PRISM data has recently been applied over a much broader region including the study area to study the spatiotemporal variability of the precipitation-dipole transition zone in the western United States associated with the El Niño Southern Oscillation (Wise, 2010). The monthly PRISM time series extend from January 1895 through June 2008. Median annual PRISM precipitation at the 36 sites ranges from less than 300 mm to more than 1200 mm. Cool-season months dominate the annual distribution of precipitation. About 90% of the annual precipitation falls in the period November–April, and the total precipitation over those months correlates highly with the total for the water-year: the median of 36 correlations (36 sites) for the period 1896–2005 is 0.98. Exploratory analysis showed that the *Q. douglassii* chronologies reach or near their highest correlation with seasonal-total precipitation for the Nov–Apr season. For brevity, in the remainder of this paper the term "precipitation" is used for the Nov–Apr total, and that interval is referred to as the "cool-season".

Several other types of climatological, hydrological, and paleoclimatic data were accessed to help interpret reconstructed droughts, wet periods and gradients in precipitation-anomaly. Composite maps of 500 mb geopotential-height anomaly from the Reanalysis data (Kalnay et al., 1996) were produced with the mapping tool provided by the NOAA/ESRL Physical Sciences Division, Boulder, Colorado (http://www.esrl.noaa.gov/psd/). Years of El Niño and La Niña events based on the Southern Oscillation Index (Redmond and Koch, 1991) were downloaded from the web site of the Western Regional Climate Center (http://www.wrcc.dri.edu/). Maps of reconstructed North America gridded Palmer Drought Severity Index (PDSI) for the expanded (286-point) network of Cook et al. (2007) were downloaded from the Drought Atlas website of Cook and Krusic (2004). Mean monthly outflow into San Francisco Bay for 1956–2005 were provided by Alan Jassby, UC Davis. These data refer to freshwater input into the northern arm of the San Francisco Estuary, and are derived from full natural flow records of rivers.

3. Methods

Each tree-ring chronology was converted to an estimate of precipitation at the tree-site by multiple linear regression (MLR) of precipitation on the chronology and its square in a distributed-lag model. The predictand for the model is the PRISM precipitation interpolated to the grid cell containing the site, and the calibration period is the overlap of the chronology with the 1896–2005 time series of precipitation. Final predictors were selected from a predictor-pool by stepwise regression. The pool includes ten variables: the chronology and squared-chronology at lags $t-2$ to $t+2$ years. Squared terms are included for flexibility to model curvilinear relationships suggested by some scatter plots of chronologies on precipitation (Fig. 2). The concave upward shape of the plots suggests the incremental change in tree-ring index for a given change in precipitation becomes less toward wetter conditions. Physically this makes sense, as the importance of additional precipitation to growth logically would decline if moisture increased to levels optimal for growth. However, the series plotted in Fig. 2 were visually judged as the strongest examples of nonlinearity among the 36 sites.

Lags were included in the model to allow for possible non-contemporaneous relationships between the annual tree-ring chronology and precipitation. Factors that could contribute to a distributed-lag response include food-storage carryover and climate-induced dieback of roots or canopy (Fritts, 1976). Lagged relationships are less likely for residual chronologies than for standard chronologies because the AR modeling used to produce residual chronologies statistically removes dependence of current year's growth on one-to-several previous years' growth (Cook, 1985). Residual chronologies are not optimally filtered as proxies for any particular climate variable, however, because climate is not explicitly included in the AR modeling. Including lags in the regression model allows for re-filtering the residual chronology to optimize the climate signal in terms of minimum error variance of predicted precipitation.

The regression model is

$$y_t = a_0 + \sum_{i=1}^{5} a_i x_{t-i+3} + \sum_{i=1}^{5} b_i x_{t-i+3}^2 + e_t \qquad (1.1)$$

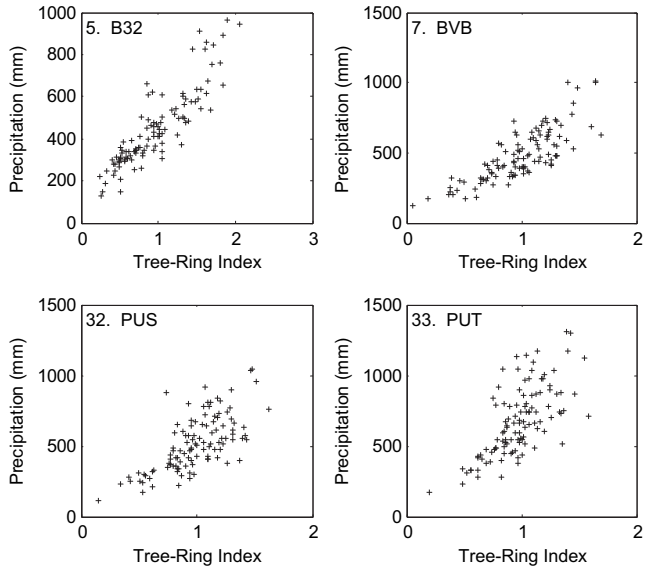

Fig. 2. Scatter plots illustrating marginally curvilinear relationships of precipitation with residual tree-ring index. Site numbers and codes as in Fig. 1 and Table 1.

where x_t is the chronology in year t; i is the lag (years); a_0, a_i, and b_i are regression coefficients; y_t is observed precipitation; and e_t is the error term. The corresponding prediction equation is

$$\hat{y}_t = \hat{a}_0 + \sum_{i=1}^{5} \hat{a}_i x_{t-i+3} + \sum_{i=1}^{5} \hat{b}_i x_{t-i+3}^2 \qquad (1.2)$$

where the caret indicates estimated value. The regression residuals, $\hat{e}_t = y_t - \hat{y}_t$, were used along with other regression quantities to compute various statistics summarizing model accuracy: root-mean-square error (RMSE), adjusted R^2 (R^2_{adj}), and p-value for significance of the overall-F of the equation (p_F). These statistics are described in standard textbooks on regression (e.g., Draper and Smith, 1981; Weisberg, 1985).

The regression scheme favors a parsimonious (simple) model, and has safeguards against overfitting. Period C is the full calibration period – full overlap of chronology with precipitation—and periods A and B are defined as the first and last halves of period C. Stepwise regression was first applied for period C to identify a suite of possible reconstruction models. The stepwise procedure was started with current year's chronology, x_t, in the model. Variables were then entered or removed at each step based on a t-test of significance of regression coefficients, with $p_{in} = 0.05$ and $p_{out} = 0.10$ (Draper and Smith, 1981). Statistics R^2_{adj}, p_F and the predictors in the model were recorded at each step. A split-sample validation (Snee, 1977) of the models identified by the initial stepwise regression was then run to identify a cutoff step and final reconstruction model. For each step, the model was calibrated on period A and validated on period B, followed by calibration on B and validation on A. The reduction-of-error statistic (RE) (Fritts et al., 1990) and validation RMSE for each half of the data were stored at each step. The final model was selected as the highest step satisfying the following conditions:

(1) Significant equation: $p_F < 0.05$ for the model calibrated on period C
(2) Positive RE of validation on periods A and B
(3) Monotonic decrease in validation RMSE over all lower steps on periods A and B

If the above three conditions were not satisfied, simple linear regression of precipitation on the chronology in year t was selected as the default model. The final selected model was then re-calibrated and cross-validated on period C, and applied to generate the multi-century reconstruction of precipitation at each site. These regression-generated predictions are referred to from here on as site-centered reconstructions. The process was repeated for each of the 36 chronologies. Because the models include lagged predictors over a possible span of five years (lags $t-2$ to $t+2$), groups of five observations rather than one observation were omitted in cross-validation (Meko, 1997). Cross-validation RMSE and RE were recorded as summary statistics of prediction error and skill of the final model.

Residuals of the site-centered regression models were checked graphically and statistically for possible violation of regression assumptions. Normality was tested by the Lilliefors test (Conover, 1980). Lag-1 autocorrelation was computed and tested for significance using a normal approximation to the distribution of sample autocorrelations (Haan, 2002, p. 288)[2]. Evidence for linear trend was checked by a t-test of the significance of the slope-coefficient in a regression of residuals against time. Scatter plots of residuals on

[2] The Durbin-Watson statistic was not used because available tables of significance did not cover sample sizes greater than 100 observations.

predicted values were checked visually for evidence of diagnostic patterns that might suggest transformation of the predictand as a remedial measure (Weisberg, 1985).

Site-centered reconstructions were regionalized into time series representing precipitation-variations in North, Central and South regions. Regionalization was guided by the following constraints: regions have similar areas; each contain multiple chronologies with a strong precipitation signal; the regional series extend back to at least the mid-1500s; and the boundaries be oriented southwest–northeast − 90° to the mountains and in concordance with the prevailing storm track (Crippen, 1986). The boundaries were initially sketched in to satisfy these constraints, and were then checked for compatibility with the spatiotemporal climate variability using principal-components analysis (PCA) of the 1896–2005 site-centered (observed) precipitation at the 36 sites mapped in Fig. 1. Spatial modes of precipitation were identified by varimax rotation of the most important components as identified by an eigenvalue greater than 1.0 (Richman, 1986; Mardia et al., 1979).

The regionalized reconstruction for a region is a weighted average of the site-centered reconstructions in the region. To avoid unduly weighting the wettest sites or those with high variance of precipitation, regional reconstructions and observed series are expressed as regional *Z*-scores, or regionally-averaged standardized anomalies (e.g., Jones and Hulme, 1996). The 1896–2001means and standard deviations were used in *Z*-score computation. The observed regional *Z*-score series is computed as

$$Z_t = \frac{1}{k}\sum_{i=1}^{k}\frac{y_{t,i} - m_i}{s_i} \tag{1.3}$$

where $y_{i,t}$ is the PRISM precipitation at site i in year t; m_i and s_i are the mean and standard deviation of site-precipitation; and k is the number of sites in the region. The k sites are a subset of the 36 sites mapped in Fig. 1. The corresponding reconstructed regional *Z*-score series is

$$Z_t^* = \frac{1}{k}\sum_{i=1}^{k} w_i\frac{\widehat{y}_{t,i} - \widehat{m}_i}{\widehat{s}_i} \tag{1.4}$$

where $\widehat{y}_{t,i}$ is the site-centered reconstruction for site i in year t;$\widehat{m}_i$ and $\widehat{s}_i$are the mean and standard deviation of $\widehat{y}_{t,i}$; and k is defined as in equation (1.3). The means and standard deviations in equations (1.3) and (1.4) are computed for the same reference-period, 1896–2001. The weights w_i in equation (1.4) are proportional to the regression R^2_{adj} of the site-centered reconstruction models[3], and are constrained such that their sum over the k sites is 1.0. The weighting scheme is intended to decrease the importance to the regionally-averaged series of those tree-ring chronologies with a weak precipitation signal. Series Z_t and $Z_t^*$are referred to as observed and reconstructed regional *Z*-scores of precipitation from here on. Subsequent analysis utilized these *Z*-score series to define events (see below), but for a practical perspective the observed percentage-of-normal precipitation corresponding to *Z*-score thresholds for events was computed. The percentage-of-normal observed time series used for that assessment is

$$p_t = \frac{100}{k}\sum_{i=1}^{k}\left(\frac{y_{t,i}}{m_i}\right) \tag{1.5}$$

where the various terms are defined as in equation (1.3).

Inter-regional gradients in precipitation-anomaly were approximated in this study by differences in *Z*-scores between region-pairs (i.e., North–South, North–Central and Central–South). Because the separation-distance between any two regions is a constant, the *Z*-score difference for any region-pair is proportional to an average gradient. The strength of tree-ring signal for a regional gradient in precipitation-anomaly was summarized by the correlation of time series of ΔZ_{obs} and ΔZ_{rec}, the observed and reconstructed differences in *Z*-scores for a region-pair. Significance of correlation was judged by a *t*-test (Snedecor and Cochran, 1989), using effective sample size (Haan, 2002, p. 289) as needed to account for loss of degrees of freedom due to autocorrelation of the individual series.

The regional reconstructed *Z*-scores for North, Central and South regions were used to generate a set of logical (0 or 1) time series classifying reconstruction years into four classes: overall-dry (D), overall-wet (W), wetter-to-south (D/W) and wetter-to-north (W/D). The D event was defined as all three regions below a specified threshold *Z*-score. The threshold was arrived at iteratively: initialized at 0 and decreased at intervals of 0.001 until the D class contained 10% of the years in the long-term tree-ring record. Conversely, the W event was defined as all three regions above a specified *Z*-score threshold of precipitation. The W threshold was initialized at 0 and increased at intervals of 0.001 until the W class contained 10% of the years in the long-term record.

W/D and D/W events were defined as a large difference in reconstructed *Z*-scores in the North and South regions. The W/D event was defined a large positive difference, and the D/W event as a large negative difference. An iterative procedure analogous to that used to identify the D and W thresholds was used to find thresholds marking the 10% of years with largest positive difference or negative difference. The W/D and D/W events refer only to relative precipitation anomalies in the North and South regions and not to whether conditions are drier-than-normal or wetter-than-normal in either region. D and W events are mutually exclusive, but various other combinations of events are possible in a given year. For example, a year can be both D and W/D if all three regions are very dry but conditions are much drier in the South than in the North.

4. Results and discussion

4.1. Site-centered reconstruction

Statistics for the site-centered regression models are listed in Table 1. Seventeen of the 36 models are simple linear regressions on the chronology at lag-0. Nineteen models include at least one lagged predictor, suggesting some benefit of lags in re-capturing climatic signal that may have been inadvertently filtered out in creating the residual chronologies. Linear terms dominate over quadratic terms: all final models include the lag-0 chronology, while only one model includes the lag-0 squared-chronology. A total of ten models include squared terms at non-zero lag, but the coefficients on those terms are much smaller than on the lag-0 chronology. This result indicates any nonlinearity in the relationships between chronologies and precipitation is of minor importance to the reconstructions.

Thirty-four of the 36 sites have highly significant ($p_F < 0.001$) regression models; these models explain between 13% and 82% of the variance of site-centered precipitation. The median R^2_{adj} for all 36 models is 0.46. Validation statistics identify the two sites with insignificant overall-*F* of regression as the only two sites with no skill of cross-validation. Split-sample validation flags two additional models as suspect for failing to achieve positive validation skill (RE > 0) on both validation-halves (Table 1).

The strength of precipitation signal as measured by regression R^2_{adj} is strongly negatively correlated with mean Nov–Apr precipitation at the site ($r = -0.65$, $N = 36$, $p < 0.01$). The nine sites with

[3] Weight set to zero if adjusted R^2 negative.

Table 1
Statistics and regional groupings for site-centered reconstructions.

		Model[d]			Validation[e]			Period[f]		Region[g]	
N[a]	Code[b]	Mean[c]	Predictors	adjR^2	RE_A	RE_B	RE_{cv}	Start	End	G1	G2
1	AC2	556	1000000000	0.51	0.59	0.30	0.49	1455	2004	S	S
2	AR2	558	1010000000	0.40	0.35	0.42	0.38	1605	2003	N	.
3	B24	466	1110000000	0.53	0.44	0.49	0.50	1699	2003	C	.
4	B27	409	1000000000	0.82	0.85	0.74	0.81	1379	2003	C	C
5	B32	448	1000110010	0.81	0.85	0.74	0.80	1409	2001	C	C
6	BCC	803	1000000000	−0.01*	0.01	−0.05	−0.03	1582	2004	N	.
7	BVB	480	1000000100	0.66	0.64	0.45	0.65	1548	2004	N	N
8	CL2	639	1000000000	0.47	0.46	0.23	0.44	1620	2004	N	.
9	COE	464	1000100000	0.35	0.35	0.23	0.31	1675	2003	C	.
10	COT	639	1000000000	0.33	0.45	0.17	0.31	1649	2004	N	.
11	DEN	701	1000000010	0.39	0.40	0.35	0.35	1596	2002	S	.
12	DI2	465	1000000100	0.80	0.75	0.73	0.79	1584	2004	N	.
13	DIB	622	1010000001	0.45	0.55	0.30	0.42	1521	2002	N	N
14	DMS	540	1000001000	0.45	0.38	0.47	0	1449	2003	S	S
15	DON	430	1000000000	0.29	0.30	0.18	0.27	1531	2005	C	C
16	DYE	514	1000001000	0.18	0.20	0.03	0.15	1602	2005	N	.
17	EEL	1077	1000000100	0.25	0.21	0.18	0.22	1537	1996	x	.
18	EMP	617	1000000000	0.25	0.23	−0.16	0.18	1695	2004	C	.
19	FE2	828	1000100000	0.13	0.14	0.06	0.09	1572	2002	N	.
20	FI2	725	1000000000	0.01*	−0.06	−0.33	−0.03	1363	2004	N	N
21	FIG	756	1000000000	0.46	0.50	0.15	0.44	1293	2003	S	S
22	HAS	551	1000000000	0.56	0.61	0.38	0.54	1460	2004	C	C
23	IND	596	1000000000	0.25	0.29	0.11	0.22	1494	2003	C	C
24	JOA	363	1001000000	0.51	0.47	0.30	0.49	1710	1995	x	.
25	KAW	589	1000000000	0.41	0.44	0.29	0.40	1494	2004	S	S
26	KR2	275	1010000000	0.62	0.57	0.61	0.60	1587	2003	S	.
27	LOB	245	1000000000	0.75	0.72	0.55	0.74	1333	2004	S	S
28	MUR	540	1000000000	0.29	0.20	0.38	0.27	1532	2004	N	N
2	PN2	338	1011000000	0.68	0.72	0.48	0.66	1579	2002	C	.
30	PP2	322	1010000000	0.61	0.57	0.46	0.59	1512	2003	C	C
31	PPC	312	1000000000	0.77	0.85	0.62	0.76	1538	2004	S	S
32	PUS	516	1000000100	0.50	0.54	0.45	0.48	1729	2004	x	.
33	PUT	673	1000000110	0.51	0.52	0.39	0.49	1536	2003	N	N
34	SJR	361	1001000000	0.50	0.46	0.25	0.48	1557	2003	C	C
35	SUT	442	1000000000	0.17	0.21	0.06	0.14	1808	2004	x	.
36	TUO	829	1000000000	0.18	0.19	−0.14	0.15	1408	2005	C	C

[a] N = sequential site number.
[b] Code = Site code, as used on map in Fig. 1.
[c] Mean = Long-term observed mean Nov–Apr precipitation (mm) for the period used to calibrate the model. This period varies by site, begins with 1896, and ends between 1994 and 2003.
[d] Model: Predictors = logical indicator of lags included in regression model. The 10 digits indicate whether a predictor is in (1) or not in (0) the final model. Positions from left to right correspond to lags 0, −2, −1, +1 and +2 on residual chronology, and lags 0, −2, −1, +1 and +2 on squared residual chronology. Statistic adjR^2 = adjusted coefficient of multiple determination for the model calibrated on full overlap of precipitation and chronology (the model used for reconstruction); asterisk flags models with overall-F statistic not significant at 0.05 alpha level.
[e] Validation = reduction-of-error statistics for validation by split-sample method and by cross-validation. RE_A is for calibration on first half of data and validation on second half; RE_B is for calibration on second half of data and validation on first half; RE_{cv} is for cross-validation (leave-5-out) on the full calibration period.
[f] Period = time coverage (starting and ending years) of long-term site-centered reconstruction.
[g] Region = grouping of sites into regions for models providing coverage for 1699–2001 (G1) and 1559–2001 (G2). N, C and S refer to "North", "Central" and "South" regions. An "X" in the G1 column means chronology not used because time coverage incomplete for 1699–2001. A "." in the G2 column indicates time coverage incomplete for 1559–2001. These sites were not used in the regional reconstructions.

$R^2_{adj} > 0.60$ have mean precipitation less than 500 mm (Table 1). Though there are exceptions, the results broadly suggest that dry sites are more favorable than wet sites for a precipitation signal in this particular tree-ring data set.

The analysis of residuals pointed out instances of possible violation of regression assumptions for a few of the 36 models. The following results were obtained for tests with significance level set at $\alpha = 0.01$: eight models failed the Lilliefors test for normality of residuals; two models had significant lag-0 autocorrelation of residuals; and four models had significant positive trend in residuals. Scatter plots of residuals on predicted values suggested increased scatter toward higher predicted values of precipitation for seven models. Because the violations found were minor and found at only a few sites, it was decided not to re-do regressions with models tailored to each site (e.g., transform predictand depending on scatterplot of residuals on predicted values). Two other factors contributed to the decision. First, simultaneous evaluation of results for 36 tests raises the likelihood of chance occurrence of "significant" results. Second, some apparent problems with the models may be due to unknown inhomogeneity of the precipitation series. For example, the significant positive trend in residuals at four sites (and positive sign of slope-coefficient at 32 of 36 sites), could plausibly result from trend in PRISM precipitation induced by temporal changes in the network of climate stations contributing to the PRISM interpolation. Another possible explanation for the positive trend is that some factor other than precipitation acted over 1896–2005 to gradually reduce tree-growth below levels expected from precipitation-variations alone. These topics were beyond the scope of the present study, but are worthy of future investigation.

All except two of the 36 site-centered regression models generated at least one reconstructed precipitation value in 1557–2001 (period of subsequent analysis) outside the range of observed precipitation in the calibration period. The assumption is made in interpreting the reconstructions that the relationships estimated for the restricted range of precipitation apply to the

broader range. Regression predictions based on predictor-values outside their calibration-period range are called interpolations (Weisberg, 1985) and may be subject to additional uncertainty beyond that implied by calibration and validation statistics.

4.2. Signal for gradient in precipitation-anomaly

Sites were grouped into North, Central and South regions, as delineated by the boundaries on the map in Fig. 3, and indicated by the codes in the last two columns of Table 1. Groups G1 and G2 in those columns refer to site-centered reconstructions based on tree-ring subsets with complete time coverage for 1699–2001 and 1557–2001, respectively. The two versions of regionalized reconstructions with different start years were generated to allow testing for sensitivity of results to site coverage. The shorter version is probably more robust because it includes more sites per region, while the longer version provides time coverage into the interesting drought epoch of the late 1500s (e.g., Stahle et al., 2000). The shorter version has 32 sites[4]: 12 North, 12 Central and 8 South. The longer version has 19 sites: 5 North, 8 Central and 6 South. Each of the three regions includes a few sites with a high signal-strength for precipitation back to the 1500s (Fig. 3). The earliest site-centered reconstruction begins in 1293, but lack of very long chronologies with a strong signal in the North region dictated restricting the G2 regional grouping to start no earlier than 1557 (Table 1).

PCA of observed precipitation, 1896–2005, confirms that the regional groupings mapped in Fig. 3 are consistent with the spatiotemporal variability of site-centered observed precipitation in the study area. The three components (PCs) with eigenvalues greater than 1.0 account for a cumulative 92.4% of the precipitation variance (Fig. 4). PC1 is by far most important, accounting for 82.8% of the variance and highlighting the regional homogeneity of precipitation anomalies. PC2 accounts for 6.7% of the variance and PC3 for 2.9%. The varimax-rotated PCs show strong spatial structure (Fig. 5): rotated PC1 has mostly same-sign loadings over the study area, with highest loadings in the Central region and toward the Sierra Nevada Mountains in the North and South regions; PC2 is a north–south contrast, with all-positive loadings in the North, all-negative in the South, and a transition in the Central region; and PC3 has high loadings only toward the coast in the Central and South regions.

The weighted-averaging procedure yielded a total of six regional *Z*-score reconstructions, one for each of the two different start years in the three regions. Scatter plots and correlations indicate strong, linear relationships between observed and reconstructed regional *Z*-score series in all three regions (Fig. 6). Correlations of observed with reconstructed regional *Z*-scores are 0.81, 0.87, and 0.88 in the North, Central and South regions, respectively. The plots in Fig. 6 apply to the regional reconstructions from the relatively dense 1699–2001 tree-ring networks. Corresponding correlations for the reconstruction from the sparser 1557–2001 subsets are 0.78, 0.89, and 0.88 (plots not shown). Based on the similarity in strength of regional precipitation signal in the sparse and dense networks, the 1557–1698 portion of the earlier *Z*-score reconstruction was appended onto the 1699–2001 *Z*-score reconstruction to create a merged 1557–2001 reconstruction for subsequent use in event analysis. In evaluating the quality of the regional *Z*-score signal it is important to recognize that the extremely high regional correlations illustrated in Fig. 6 were arrived at without tuning or calibrating tree-ring data to observed precipitation beyond the initial site-centered reconstructions.

[4] Collection dates of four of the 36 chronologies are too early to allow site-centered reconstructions to 2001 (Table 1).

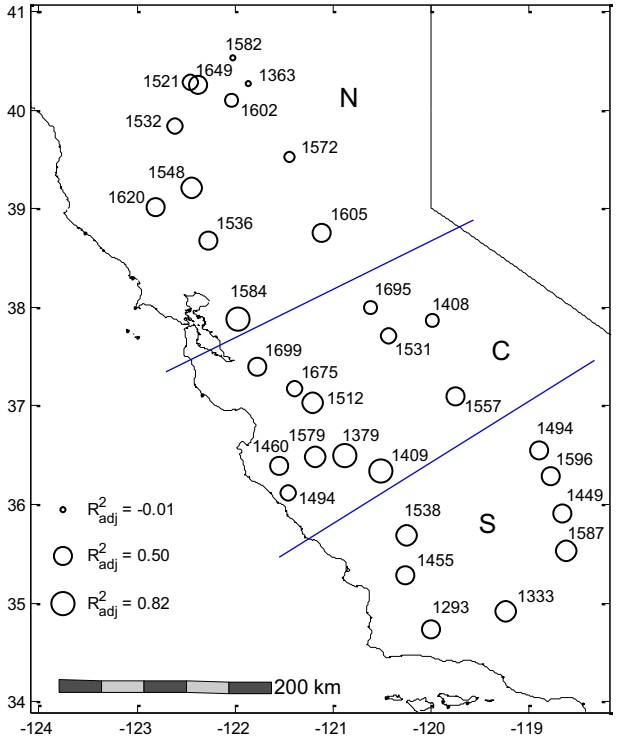

Fig. 3. Map showing regional grouping of tree-ring sites and strength of precipitation signal. Symbols sized proportional to R^2_{adj} for site-centered regression (Table 1). Numbers beside symbols are start years of site-centered reconstructions.

The extreme positive and negative inter-regional differences in *Z*-score precipitation, 1557–2001, for the merged *Z*-score reconstructions are listed in Table 2. Extremes are greatest for the difference of North and South, but are substantial for the more closely spaced North–Central and Central–South pairs. The 20th century is represented in the extremes by only 1939, when the negative *Z*-score indicates a wetter-to-south pattern. With rare exception (fewer than 10% of years) a large difference in *Z*-score in the North and South regions was found to be accompanied by an intermediate *Z*-score in the Central region. In such years the average gradient, though proportional to the difference of North

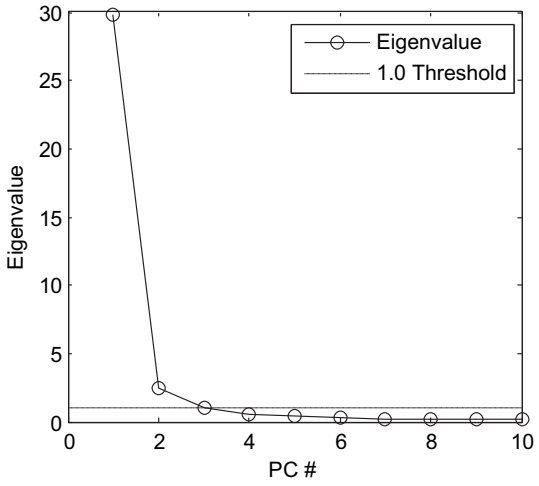

Fig. 4. Scree plot of eigenvalue against principal-component number for PCA of November–April precipitation at 36 tree-ring sites. Eigenvalues for the first three components exceed 1.0. Analysis period 1896–2005.

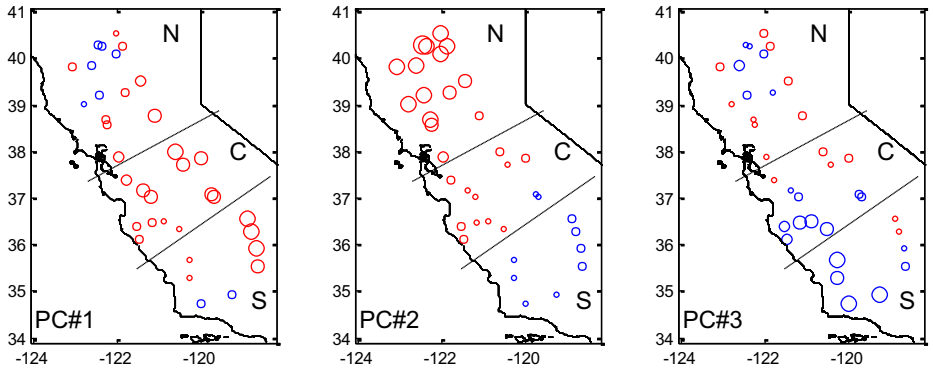

Fig. 5. Loadings maps for first three rotated principal-components of cool-season (Nov–Apr) precipitation at 36 tree-ring sites. Sites listed in Table 1. Size of symbols proportional to magnitude of loading; color indicates positive (red) or negative (blue) sign. Region boundaries as in Fig. 3. (For interpretation of the references to colour in this figure legend, the reader is referred to the web version of this article).

and South *Z*-scores, actually reflects a much stronger gradient at a finer spatial scale between two adjacent regions and a flat or reversed gradient between the other two regions.

At the widest regional spacing (North–South), the reconstructed difference-series tracks the observed difference-series at high and low frequencies (Fig. 7A). High-frequency tracking is illustrated by the same direction of year-to-year change for 28 consecutive years from 1916 to 1943. Low-frequency tracking is illustrated by synchronous multi-year positive departures (wetter-to-north) in 1931–1933, 1943–1945 and 1976–1978; and negative departures (wetter-to-south) in 1925–1928, 1959–1961 and 1970–1973. Scatter plots for the two series plotted in Fig. 7A show a highly significant signal ($r = 0.67, N = 106, p \ll 0.01$) for a North–South difference in precipitation-anomaly (Fig. 7B). The signal is noisy, however, and equivalent to only about 46% of the variance explained in linear regression. The noise is manifested in the time series plots of Fig. 7A by large differences in the reconstructed and observed departures from zero in some years (e.g., 1909–1915, 1957, 1982, and 1995). The challenge to accurately reconstructing gradients in precipitation-anomaly is especially great in this study area because of the strong spatial coherence of cool-season precipitation anomalies. The coherence, evident in the overwhelming importance of PC1 in the PCA of observed the precipitation (Figs. 4 and 5), is reflected by the high correlation of observed *Z*-score precipitation in the North and South regions (Fig. 7C). The challenge increases with closer spacing of regions. For example, analogous plots (not shown) to Fig. 7B for North–Central and Central–South differences show somewhat noisier relationships and smaller – though still highly significant – correlations: r=0.59 for North–Central and $r = 0.53$ for Central–South.

4.3. Event analysis

The reconstruction *Z*-score thresholds for W, D, W/D and D/W events are listed in Table 3 along with equivalent thresholds of observed percentage-of-normal precipitation. An example will serve to illustrate the interpretation of the last column of Table 3. Consider W events, defined as all three regions with reconstructed regional *Z*-score greater than 0.60. This threshold yields exactly 13 W events in 1896–2001. If the North, South and Central observed regional percentage-of-normal precipitation series from equation (1.5) are analyzed iteratively to find the numbers of years in the period 1896–2001 for which all three series are above some specified threshold percentage-of-normal, a threshold of 129.9% of normal marks exactly 13 years. The percentage thresholds in the last column in Table 3 are offered as practical yardsticks for a perspective on the less-intuitive *Z*-score thresholds used to define events.

Event-occurrence varies greatly over centuries and shorter intervals (Fig. 8). W and D events dominate the series over the last 30 years. The expected number of events per century by chance is 10: the thresholds by definition classify 44 years in the period 1557–2001 (10% of the years) as events for each event-type. The 20th century, with 13, 12, 10 and 8 events of type W, D, W/D and D/W, is high in W and D events and low in D/W events relative to expectation (Fig. 8). These tendencies of the recent segment of the reconstruction are also evident in cumulative distribution functions of the numbers of events in 50-yr and 100-yr sliding time windows (Fig. 9). For example, the 0.90 non-exceedance probability marked by the circle in the upper-left plot indicates that the seven W events in the most recent 50-yr period (1952–2001) is greater than the

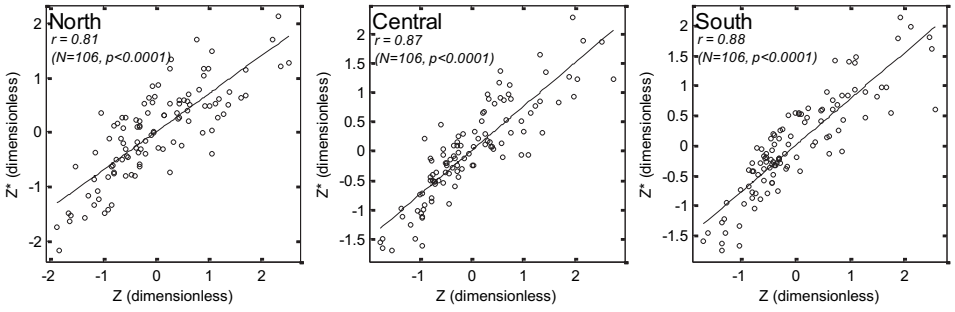

Fig. 6. Scatter plots illustrating relationship between reconstructed and observed regional-average *Z*-scores of precipitation. Reconstructed series (Z^*) is plotted against observed series (Z) for North, Central and South regions. Straight line is fitted linear regression. Correlation coefficient, sample size and *p*-value for significance of correlation (two-tailed test) annotated at upper left. Analysis period for regression is 1896–2001. Series Z^* are from 1699 to 2001 subsets of tree-ring sites.

Table 2
Extreme inter-regional difference[a] in reconstructed *Z*-score precipitation, 1557–2001.

	Negative		Positive	
Region-Pair	ΔZ^*	(Year)	ΔZ^*	(Year)
North–South	−1.68	(1939)	1.88	(1879)
North–Central	−1.46	(1615)	1.59	(1643)
Central–South	−1.32	(1816)	1.08	(1641)

[a] Entries are the largest positive and negative differences of regionally-averaged reconstructed *Z*-score precipitation as given by equation (1.4). Reconstructed *Z*-scores before 1699 from the sparse tree-ring network.

Table 3
Precipitation thresholds marking events.

Threshold			
Event[a]	*Z*-score[b]	*N*[c]	Pctg[d]
W	0.60	13	129.9
D	−0.62	13	74.7
W/D	0.88	10	32.6
D/W	−0.82	9	−29.2

[a] Event_type: W = overall-wet, D = overall-dry, W/D = wetter-to-north, D/W = wetter-to-south.
[b] Threshold *Z*-score (W and D),or north–south difference in *Z*-score (W/D and D/W) of reconstructed regional precipitation defining events.
[c] Number of events in period 1896–2001.
[d] Percentage-of-normal threshold identifying same number of events (N) in 1896–2001 record of observed regional precipitation.

number of W events in about 90% of the 396 overlapping 50-yr periods from 1557 to 2001.

The extreme example of clustering in the event time series is the 1780–1790s: six of the nine years 1784–1792 are classified as W; this wet interval is bracketed by pairs of consecutive D years. The only run longer than two years for any event-type is a three-year run of D/W events in 1816–1818. With the exception of the 18th century, consecutive years of any event-type happen at most once or twice per century. The two-year run of D events in 1579–1580 coincides with the lowest reconstructed annual flows of the Sacramento River since A.D. 869 (Meko et al., 2001), but otherwise the late-1500s event series for the Central Valley does do not bear an imprint of the late-1500s megadrought that affected much of western North America (Stahle et al., 2000). The frequent W/D (wetter-to-north) events in the last two decades of the 1500s are consistent, however, with the extreme drought at the time in the southwestern United States, Colorado River Basin and northern Mexico (Stahle et al., 2000, 2009; Grissino-Mayer 1996; Meko et al., 1995).

Given the size of the study area and restrictiveness of the thresholds it is reasonable to expect the event series to be related in some way to anomalies in large-scale circulation of the atmosphere. The composite cool-season 500 mb height-anomaly map for the five most severe D events in the period 1949–2001 has a band of elevated heights extending from the Pacific Ocean into the Pacific Northwest (Fig. 10, left). The high pressure favors drought through subsidence, suppression of development of storms, and blocking of movement of storms into the study area. Moreover, the anomalous flow across the study area associated with the height anomalies is from the continent to the ocean – a pattern opposing advection of moist air from the Pacific. Some individual years depart strongly from the composite. In D years 1977 and 1987, for example, the anomalous high is cellular rather than zonally elongated and is shifted onto the continent. The 1977 anomalous high is centered directly on the Pacific Northwest coast.

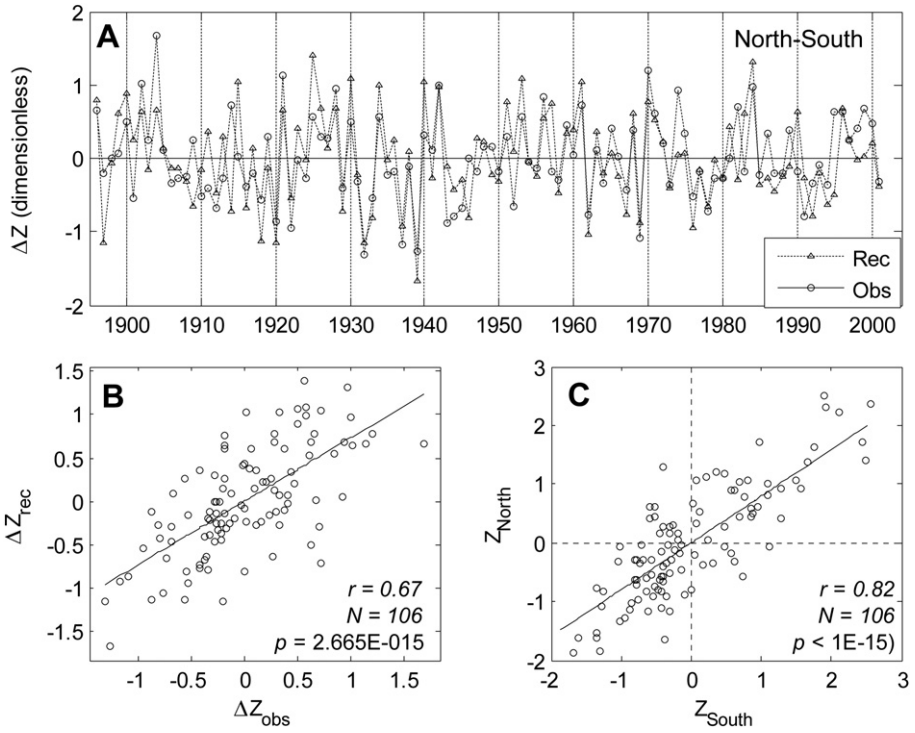

Fig. 7. Time plot and scatter plots illustrating tree-ring signal for precipitation-anomaly gradient. A) Time plots of reconstructed and observed difference in *Z*-score precipitation in North and South regions, 1896–2001. B) Scatterplot of reconstructed against observed difference in *Z*-score precipitation in North and South regions. C) Scatterplot of observed *Z*-score precipitation in North against observed *Z*-score precipitation in South. Analysis period for scatter plots is 1896–2001. ΔZ_{rec} is the difference in regional *Z*-score reconstructed precipitation in North and South regions. ΔZ_{obs} is the corresponding difference in observed precipitation. Straight lines in (B) and (C) are least-squares fits; the correlation coefficient, sample size, and *p*-value for at two-tailed test of significance of correlation are annotated. Reconstructed series in (A) and (B) are from 1699 to 2001 subsets of tree-ring sites.

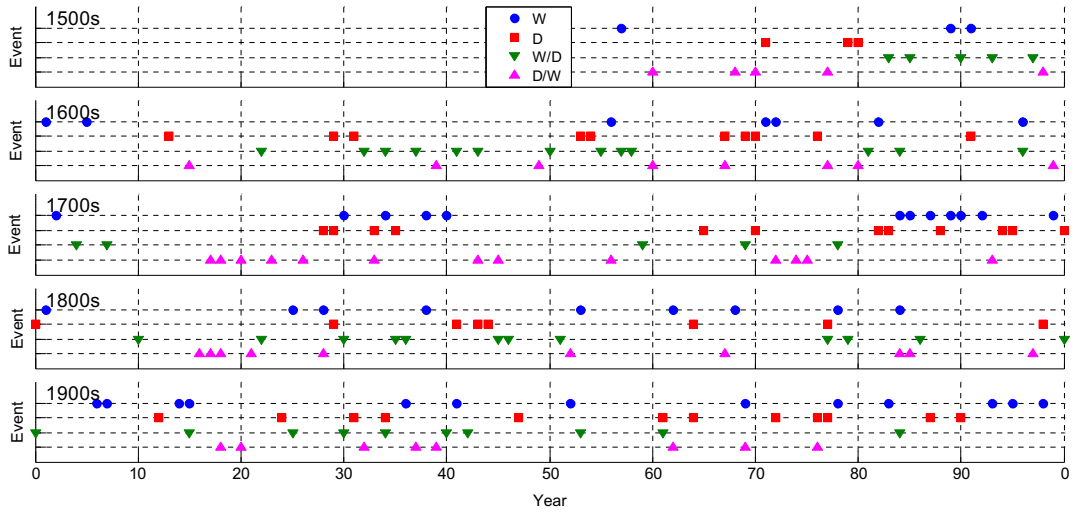

Fig. 8. Time series of events, 1557–2000. Codes D and W refer to all regions dry and all regions wet. Code W/D is strong contrast with wetter in North region than in South region. Code D/W is strong contrast with wetter in South region than in North region. Thresholds defined (see Section 3, Table 2) such that 10 percent of the years in the period 1557–2001 are classified into each event-type. Event time series cover 1557–2001, but plot truncated because no events in 2001.

In a case study of the 1977 drought, Namias (1978a) theorizes the persistent height anomalies during the drought were favored by an atmospheric flow pattern in phase with the normal winter pattern but greatly amplified.

The composite for W years is broadly the reverse of that for D years, at least in the immediate vicinity of the study area: an anomalous low protrudes from the Pacific onto the continent (Fig. 10, right). The same factors mentioned for the D events would operate in the opposite sense to favor moist conditions over the study area. The W event is the only one of the four event-types to show a strong association with El Niño or La Niña: the five W years mapped in Fig. 10 coincide with strong or moderate El Niño events as classified by the Southern Oscillation Index (SOI) (Redmond and Koch, 1991). Moreover, seven of the nine W years in the complete overlap period (1934–2001) of the reconstructions and SOI-based index are El Niño years.

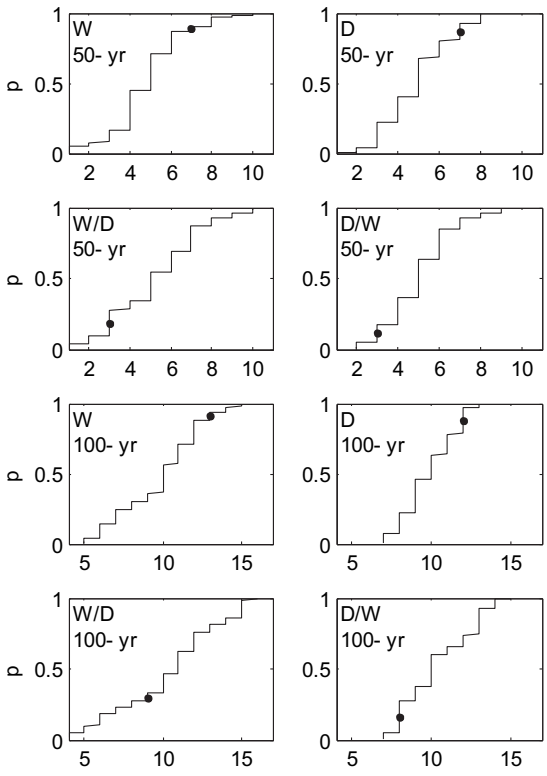

Fig. 9. Empirical cumulative distribution functions showing long-term context of frequency of events in most recent 50 and 100 years. Non-exceedance probability for most recent period, ending in 2001, marked by dot. Top four plots show results for 50-yr window, and bottom four plots for 100-yr window. Events coded as overall-wet (W), overall-dry (D), wetter-to-north (W/D) and wetter-to-south (D/W).

The D/W 500 mb composite comprises just three years and poorly represents its constituent years (Fig. 11, left). A strong anomalous low is centered along the Pacific Northwest coast and low geopotential-heights blanket western North America from southern Alaska to southern Mexico in 1969. In 1976, anomalously low heights at low and high latitudes are split by a zonally-oriented band of elevated or normal heights at mid-latitudes. The anomaly-pattern is strongly meridional in 1969 and strongly zonal in 1976. Another unusual aspect of the 1969–1976 pair is that both years also qualify as other event-types: 1969 as W and 1976 as D (Fig. 8). Years in multiple classes are rare in the 1557–2001 record: 11 cases in the 165 years with an event of any type. The winter (DJF) of 1975–1976 was characterized by less than 100% of normal precipitation over much of California, and a belt of less than 50% of normal precipitation extending across the north half of the state, through northern Nevada up to the Nevada-Utah border (Namias, 1978b). That substantial wetter-to-south gradients in precipitation-anomaly can occur with either extreme drought or wetness over California precludes identification of "characteristic" atmospheric circulation anomaly-types for D/W events.

Of the four event-types, the W/D composite perhaps best represents its individual years. This composite shows a strengthened Aleutian low, and a band of anomalous high pressure, generally veering in a southwest–northeast direction across California. The orientation of the anomalous high favors stronger off-continent flow (away from the moisture source) in southern California than in northern California, and blocking of storms from the Pacific off central and southern California.

The high frequency of W and D events relative to D/W and W/D events in the last 25 years of record (1977–2001) follows a post-1976 shift of the atmosphere-ocean climate system over the North Pacific Ocean (Miller et al., 1994). Two reported characteristics of the shift are a strengthened Aleutian Low and a southerly shift of

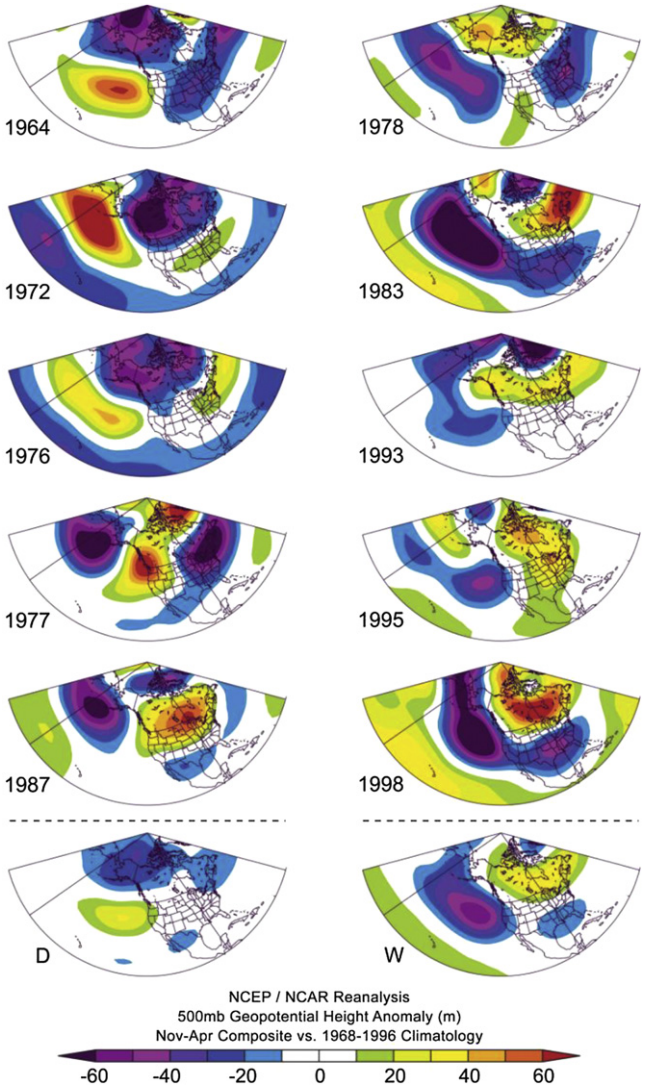

Fig. 10. Cool-season (Nov–Apr) 500 mb geopotential-height anomalies and composites for D and W events (left and right columns, respectively). Composites at bottom and individual years above. Seven W events and seven D events occur in the overlap of reconstruction with height data (1949–2001), but for brevity plotted maps are restricted to the five most extreme events. Height-anomaly data from Reanalysis (Kalnay et al., 1996).

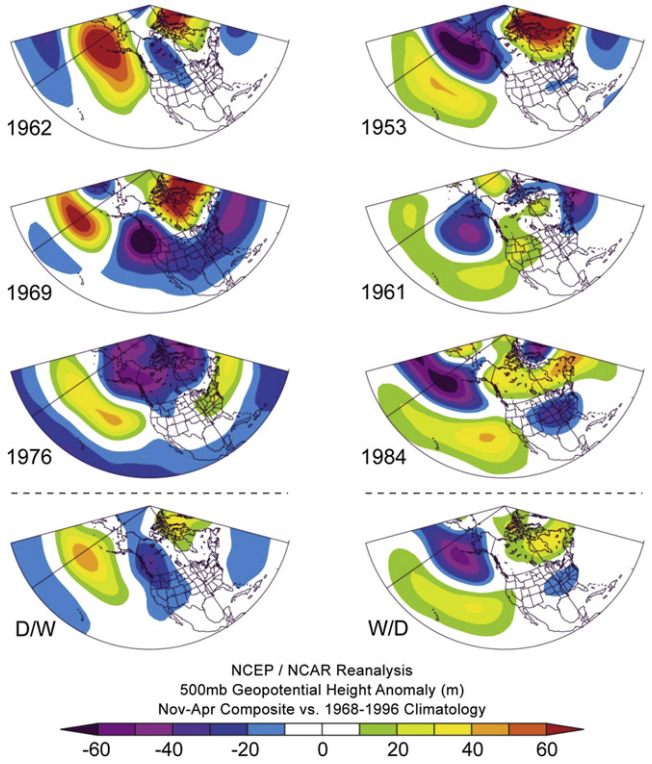

Fig. 11. Cool-season (Nov–Apr) 500 mb geopotential-height anomalies and composites for D/W and W/D events (left and right columns, respectively). Remainder of caption follows Fig. 10.

storm track in western North America (Miller et al., 1994). A strengthened Aleutian low is characteristic of several of the strongest D and W events (Fig. 10). That a southerly-displaced storm track leads to an increase in W rather than D/W events in study area probably indicates the shifting storm track has affected moisture delivery on a larger scale than these individual regions; uniformly increased precipitation over much of California would leave no record in D/W events.

Interpretation of regional dendroclimatic studies in North America can benefit from the large-scale perspective supplied the North America Drought Atlas (Cook et al., 2007). One example is presented here by drawing on the Atlas for insight into the large-scale moisture-anomaly patterns associated with the unique three-year sequence of D/W events in 1816–1818 (see Fig. 8). This sequence is of interest not only because it is the sole run of more than two years of any event-type, but because the D/W event-type is conspicuously absent since 1976 (Fig. 8). The Atlas shows that 1816, 1817 and 1818 share the common feature of wet conditions across Mexico (Fig. 12). The entire USA west of the Great Plains was extremely wet in 1816, a year in which the D/W pattern in California is clearly embedded in a larger-scale gradient from Mexico to the Pacific Northwest. The map for 1817 suggests a moderating of the overall wetness and shrinkage of the wet core toward Mexico. The map for 1818 shows further shrinkage of the wetness to central Mexico and development of severe drought in the interior Southwest. The D/W event in 1818 appears to be a relatively small-scale contrast between a finger of that drought extending across northern California and a pocket of wetness in central/southern California.

The 1816–1818 D/W run occurs immediately after the 1815 eruption of Tambora, considered by some the most violent explosive volcanic eruption of the Holocene (Bradley and Jones, 1992). In terms of stratospheric loading, Tambora was likely a much stronger volcano than Pinatubo (Bradley and Jones, 1992; Stenchikov et al., 2007). GCM simulations and observations suggest the climate signal of such eruptions may be difficult to distinguish from that of El Niño (Robock, 2000; Stenchikov et al., 2007). The wetness across Mexico in 1816–1818 (Fig. 12) is consistent with El Nino, but the idealized contrast of dry Pacific Northwest and wet Southwest (Wise, 2010) is evident only in 1817. Moreover, as pointed out previously, W events – not D/W events – have a high frequency of co-occurrence with El Niño events. In fact, none of the five D/W events recorded since 1934 (Fig. 8) match El Niño years. The D/W events lack an El Niño signal because the complete spatial domain of the tree-ring network is south of the latitude separating opposite-sign moisture responses to El Niño (e.g., Wise, 2010). The coincidence of the 1816–1818 run of D/W events and Tambora is interesting and deserving of further study, but any attribution of cause-and-effect is as yet speculative.

The proximity of the tree-ring network to major runoff-producing areas in the Sierra Nevada Mountains leads to a strong relationship between W and D events and inflow to the San Francisco Estuary. For example, February–June inflow averages 90,143 m^3/s for the five

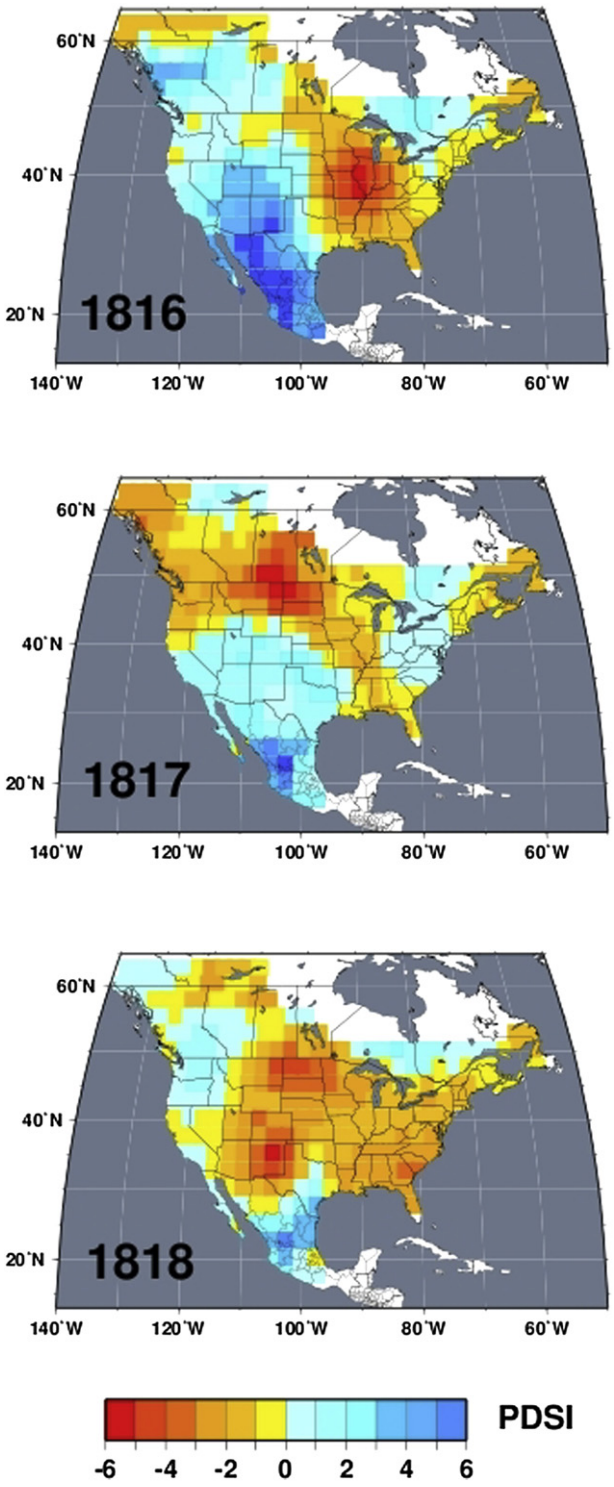

Fig. 12. Reconstructed gridded Palmer Drought Severity Index for three D/W years in early 1800s. Maps generated online with mapping tool at Drought Atlas website (Cook and Krusic, 2004).

strongest W events since 1956 and 12,539 m3/s for the five strongest D events (years in left and right panels of Fig. 10). These averages correspond to more than twice and less than one-third the mean (1956–2003) inflow of 39,888 m3/s. W/D and D/W events are likewise probably associated with north–south contrasts in runoff anomalies in tributaries of the Sacramento and San Joaquin Rivers, but that analysis is beyond the scope of this paper.

5. Conclusion

The *Q. douglasii* tree-ring network used in this study has a statistically significant signal for gradients in cool-season precipitation-anomaly along the Central Valley of California. This finding bodes well for future climatological and hydrologic studies in California requiring long-term finely-resolved spatial data on moisture anomalies. Potential applications include studying long-term variations in storm tracks, and in tendencies for compensating runoff anomalies in different watersheds. Tree-ring information such as presented here could also be useful in signal-detection of effects of greenhouse-related climate change – if, for example, an expected effect is amplified drying toward the southerly latitudes. More studies are needed to confirm the generality utility of tree-ring networks for detecting subtle spatial shifts in moisture anomalies. Obvious requirements are 1) significant spatial gradients in anomalies of seasonal precipitation across the study area, 2) strong sensitivity of tree-growth to precipitation in a particular season, and 3) sampling of the study area by a sufficiently dense network of tree-ring chronologies.

Analysis of gradients in precipitation-anomaly on a finer scale than addressed in this paper may be possible, but may be problematic for lack of a dense network of long-term climate records. This limitation cannot be circumvented with high-resolution interpolated climate data sets (e.g., PRISM) because those data sets ultimately rely on station data. Use of interpolated climate data may actually exacerbate the difficulty of detecting a real precipitation-anomaly gradient between two locations because of spatial smoothing of the precipitation anomalies. In view of this problem and the remarkably high inter-regional correlation of cool-season precipitation in the Central Valley, it is encouraging that the *Q. douglasii* network yields a statistically significant signal for precipitation-anomaly gradients even between adjacent regions (e.g., Central and South).

Acknowledgements

Funding was provided by the CALFED Ecosystem Restoration Program. We thank Matthew D. Therrell, Jesse R. Edmondson, Dorian J. Burnette, and Laurie N. Stahle for their assistance in chronology development. We also thank the many private landowners and public land managers who permitted tree-ring sampling on their private property.

Appendix A. Supplementary Data

Supplementary data includes a detailed description of development of the tree-ring chronologies; time series of residual tree-ring chronologies and site-interpolated PRISM precipitation; and various derived and reconstructed time series discussed in this paper.

References

Baldwin, J.L., 1973. Climates of the United States. NOAA, U.S. Department of Commerce, Washington, D.C., pp 113.
Bradley, R.S., Jones, P.D., 1992. Records of explosive volcanic eruptions over the last 500 years. In: Bradley, R.S., Jones, P.D. (Eds.), Climate since A.D. 1500. Routledge, New York, pp. 606–622.
Cayan, D.R., 1996. Interannual climate variability and snowpack in the western United States. Journal of Climate 9, 928–948.
Conover, W., 1980. Practical Nonparametric Statistics, second ed. John Wiley & Sons, New York.
Cook, E.R., 1985. A time series approach to tree-ring standardization. Unpublished PhD Thesis, University of Arizona, Tucson, Department of Geosciences.
Cook, E.R., Krusic, P.J., 2004. The North American Drought Atlas. Lamont-Doherty Earth Observatory and the National Science Foundation. http://iridl.ldeo.columbia.edu/SOURCES/.LDEO/.TRL/.NADA2004/.pdsi-atlas.html (Accessed 29.07.10).

Cook, E.R., Meko, D.M., Stahle, D.W., Cleaveland, M.K., 1999. Drought reconstructions for the continental United States. Journal of Climate 12, 1145–1162.
Cook, E.R., Seager, R., Cane, M.A., Stahle, D.W., 2007. North American drought: reconstructions, causes, and consequences. Earth-Science Reviews 81, 93–134.
Cook, E.R., Shiyatov, S., Mazepa, V., 1990. Estimation of the mean chronology. In: Cook, E.R., Kairiukstis, L.A. (Eds.), Methods of Dendrochronology, Applications in the Environmental Sciences. Kluwer Academic Publishers, Dordrecht, pp. 123–132.
Cook, E.R., Woodhouse, C.A., Eakin, C.M., Meko, D.M., Stahle, D.W., 2004. Long-term aridity changes in the western United States. Science 306, 1015–1018.
Crippen, J.R., 1986. California; surface-water resources. United States Geological Survey Water-Supply Paper 2300. In: Moody, D.W., Chase, E.B., Aronson, D.A., (Compilers) (Eds.), National Water Summary 1985 – Hydrologic Events and Surface-Water Resources. United States Government Printing Office, Washington, DC, pp. 157–166.
Daly, C., Gibson, W.P., Taylor, G.H., Johnson, G.L., Pasteris, P., 2002. A knowledge-based approach to the statistical mapping of climate. Climate Research 22, 99–113.
Daly, C., Halbleib, M., Smith, J.I., Gibson, W.P., Doggett, M.K., Taylor, G.H., Curtis, J., Pasteris, P.P., 2008. Physiographically-sensitive mapping of temperature and precipitation across the conterminous United States. International Journal of Climatology 28 (15), 2031–2064.
Dettinger, M.D., Cayan, D.R., Diaz, H.F., Meko, D.M., 1998. North-south precipitation patterns in western North America on interannual-to-decadal timescales. Journal of Climate 11, 3095–3111.
Draper, N.R., Smith, H., 1981. Applied Regression Analysis, second ed. John Wiley & Sons, Inc., New York, pp 709.
Douglass, A.E., 1941. Crossdating in dendrochronology. Journal of Forestry 39, 825–831.
Fritts, H.C., 1976. Tree Rings and Climate. Academic Press, London, pp 567.
Fritts, H.C., 1991. Reconstructing Large-Scale Climatic Patterns from Tree-Ring Data: A Diagnostic Analysis. University of Arizona Press, Tucson, pp 286.
Fritts, H.C., Guiot, J., Gordon, G.A., 1990. Verification. In: Cook, E.R., Kairiukstis, L.A. (Eds.), Methods of Dendrochronology, Applications in the Environmental Sciences. Kluwer Academic Publishers, Dordrecht, pp. 178–185.
Gibson, W.P., Daly, C., Kittel, T., Nychka, D., Johns, C., Rosenbloom, N., McNab, A., Taylor, G., 2002. Development of a 103-year high-resolution climate data set for the conterminous United States. In: Proc., 13th AMS Conf. on Applied Climatology. Amer. Meteorological Soc., Portland, OR, pp. 181–183. May 13–16.
Grissino-Mayer, H.D., 1996. A 2129-year reconstruction of precipitation for northwestern New Mexico, USA. In: Dean, J.S., Meko, D.M., Swetnam, T.W. (Eds.), Tree Rings, Environment and Humanity: Proceedings of the International Conference, Tucson, Arizona, 17–21 May 1994. Radiocarbon, Tucson, pp. 191–204.
Grissino-Mayer, H.D., 2001. Evaluating crossdating accuracy: a manual and tutorial for the computer program COFECHA. Tree-Ring Research 57, 205–221.
Griffin, R.D., 2007. A 600-Year Streamflow History in the Salinas Valley Reconstructed from Blue Oak Tree Rings. Unpublished MS Thesis. University of Arkansas, Department of Geosciences, 67 pp.
Haan, C.T., 2002. Statistical Methods in Hydrology, second ed. Iowa State University Press, Ames, Iowa.
Holmes, R.L., 1983. Computer-assisted quality control in tree-ring dating and measurement. Tree-Ring Bulletin 43, 69–78.
Holmes, R.L., Adams, R.K., Fritts, H.C., 1986. Tree-Ring Chronologies of Western North America: California, Eastern Oregon, and Northern Great Basin, Including Users Manuals for Computer Programs COFECHA and ARSTAN. available from. In: Chronology Series, vol. VI. Laboratory of Tree-Ring Research, Bldg 58, University of Arizona, Tucson, Arizona. 85721182.
Hughes, M.K., Kelly, P.M., Pilcher, J.R., LaMarche Jr., V.C. (Eds.), 1982. Climate from Tree Rings. Cambridge University Press, p. 223.
(Preparer) Jones, J., 2008. California Drought, an Update. State of California, The Water Resources Agency, Dept. of Water Resources, California.
Jones, P.D., Hulme, M., 1996. Calculating regional climatic time series for temperature and precipitation: methods and illustrations. International Journal of Climatology 16, 361–377.
Kalnay, E., Kanamitsu, M., Kistler, R., Collins, W., Deaven, D., Gandin, L., Iredell, M., Saha, S., White, G., Woollen, J., Zhu, Y., Chelliah, M., Ebisuzaki, W., Higgins, W., Janowiak, J., Mo, K.C., Ropelewski, C., Wang, J., Leetmaa, A., Reynolds, R., Jenne, R., Joseph, D., 1996. The NCEP/NCAR reanalysis 40-year project. Bulletin American Meteorological Society 77, 437–471.
Mardia, K., Kent, J., Bibby, J., 1979. Multivariate Analysis. Academic Press, pp 518.
Meko, D.M., 1997. Dendroclimatic reconstruction with time varying subsets of tree indices. Journal of Climate 10, 687–696.
Meko, D.M., Stockton, C.W., Boggess, W.R., 1995. The tree-ring record of severe sustained drought. Water Resources Bulletin 31 (5), 789–801.
Meko, D.M., Therrell, M.D., Baisan, C.H., Hughes, M.K., 2001. Sacramento River flow reconstructed to A.D. 869 from tree rings. Journal of the American Water Resources Association 37 (4), 1029–1040.
Miller, A.J., Cayan, D.R., Barnett, T.P., Graham, N.E., Oberhuber, J.M., 1994. The 1976–1977 climate shift of the Pacific Ocean. Oceanography 7 (1), 21–26.
Namias, J., 1978a. Multiple causes of the North American abnormal winter, 1976–1977. Monthly Weather Review 106 (3), 279–295.
Namias, J., 1978b. Recent drought in California and western Europe. Reviews of Geophysics and Space Physics 16 (3), 435–458.
Redmond, K.T., Koch, R.W., 1991. Surface climate and streamflow variability in the western United States and their relationship to large-scale circulation indices. Water Resources Research 27, 2381–2399.
Richman, M.B., 1986. Rotation of principal components. Journal of Climatology 6, 293–335.
Robock, A., 2000. Volcanic eruptions and climate. Reviews of Geophysics 38 (2), 191–219.
Snedecor, G.W., Cochran, W.G., 1989. Statistical Methods, eighth ed. Iowa State University Press, Ames, Iowa, pp 803.
Snee, R.D., 1977. Validation of regression models: methods and examples. Technometrics 19, 415–428.
Stahle, D.W., Cook, E.R., Cleaveland, M.K., Therrell, M.D., Meko, D.M., Grissino-Mayer, H.D., Watson, E., Luckman, B.H., 2000. Tree-ring data document 16th century megadrought over North America. EOS Transactions 81 (12), 121–125.
Stahle, D.W., Cook, E.R., Villanueva Diaz, J., Fye, F.K., Burnette, D.J., Griffin, R.D., Acuña-Soto, R., Seager, R., Heim Jr., R.R., 2009. Recent drought in Mexico. EOS, Transactions 90, 89–99.
Stahle, D.W., Griffin, R.D., Cleaveland, M.K., Edmondson, J.R., Fye, F.K., Burnette, D.J., Abatzoglou, J.T., Redmond, K.T., Meko, D.M., Dettinger, M.D., Cayan, D.R., Therrell, M.D. Tree-ring reconstruction of the salinity gradient in the northern estuary of San Francisco Bay. San Francisco Estuary & Watershed Science, in press.
Stahle, D.W., Therrell, M.D., Cleaveland, M.K., Cayan, D.R., Dettinger, M.D., Knowles, N., 2001. Ancient blue oaks reveal human impact on San Francisco Bay salinity. EOS, Transactions, American Geophysical Union 82 (12).
Stenchikov, G., Ramaswamy, V., Delworth, T., 2007. Impact of Big Tambora Eruption on ENSO, Ocean Heat Uptake, and Sea Level. Abstract #PP31E-07. American Geophysical Union. Fall Meeting 2007.
Stockton, C.W., Boggess, W.R., Meko, D.M., 1985. Climate and tree rings. In: Hecht, A.D. (Ed.), Paleoclimate Analysis and Modeling. John Wiley & Sons, New York, pp. 71–150.
Stokes, M.A., Smiley, T.L., 1996. An Introduction to Tree-Ring Dating. University of Arizona Press, Tucson, pp 73.
Weisberg, S., 1985. Applied Linear Regression, second ed. John Wiley, New York. pp 324.
Wise, E.K., 2010. Spatiotemporal variability of the precipitation dipole transition zone in the western United States. Geophysical Research Letters 37 (L07706). doi:10.1029/2009GL042193 2010.